# Numerical Modelling of Infragravity Wave Response during Delilah

Report submitted to RIKZ

Ap van Dongeren and Ad Reniers

Report 10-99

TUDelft

Delft University of Technology
Hydromechanics Section

# Numerical Modelling of Infragravity Wave Response during Delilah

**Ap Van Dongeren[12] and Ad Reniers[1]**

**ABSTRACT:** *In this paper the nonlinear numerical model SHORECIRC is applied to simulate the infragravity wave conditions on two days during the 1990 Delilah campaign. In order to simulate the wave conditions an algorithm has been derived which synthesizes a directional offshore wavefield from data including the bound, directional low-frequency components. The model-data comparison shows that the mean short wave transformation on the real bathymetry is predicted correctly, and that the mean longshore current is predicted very well for one of the two days without tuning the parameters. Furthermore, the structure of the infragravity spectrum as measured in the nearshore array is correctly represented but the energy level is underestimated.*

[1]Section of Fluid Mechanics, Dept. of Civil Engineering, Delft University of Technology, Stevinweg 1, 2628 CN Delft, The Netherlands.

[2]Presently at: Division MCI, WL|Delft Hydraulics, P.O. Box 177, 2600 MH Delft, The Netherlands. fax: +31-15-285-8712. corresponding email: Ap.vanDongeren@wldelft.nl

# 1 Introduction

It is well-established that short waves ($\mathcal{O}(10^{-1})Hz$) incident on a beach force longer-period waves ($\mathcal{O}(10^{-2})Hz$) which are released from the shortwave groups in the shoaling and breaking process. These long waves reflect off the beach, propagate seaward and may become trapped on the coastline as an edge wave or propagate out to deeper water as a leaky wave. The total motion of the incoming and outgoing long waves produces a standing wave-like pattern which was called "surf beats" by Munk (1949) and Tucker (1950), who were the first to report field measurements of this phenomenon.

Later, these low-frequency motions became known as "infragravity waves" and were confirmed in a number of field campaigns (Wright *et al.*, 1979, 1982; Huntley *et al.*, 1981; Holman, 1981; Guza & Thornton, 1982, 1985; Oltman-Shay & Guza, 1987; Howd *et al.*, 1991) to contain a significant portion of the total energy in the wave field, especially in shallower water. Therefore, these waves may have an important effect on the nearshore morphology.

Longuet-Higgins & Stewart (1962, 1964) showed from theoretical considerations that a bound long wave propagates with the short waves at their group velocity in water of constant depth, and suggested that this bound wave is released as a free wave.

Gallagher (1971) and Foda & Mei (1982) showed that difference-frequency interactions of pairs of short-wave components could excite the growth of edge waves. Recently, Lippmann *et al.* (1997) examined the initial growth rate of such edge waves for the fully resonant case and Chen & Guza (1998, 1999) studied the back-scattering effect of periodic topographic variations.

Symonds *et al.* (1982) developed a model in which the groupiness which existed outside the breaker zone is destroyed by the breaking assuming that the short waves inside the surf zone will decay with a saturated wave height. This implies that the position of the break point varies over the period of the wave group because higher waves in the group will break further offshore than lower waves. The time-varying break point then acts as a wave maker, inducing a slow variation of the set up and generating long waves at the frequency of the break point oscillations, which is equal to the frequency of the short-wave groups.

Schäffer & Svendsen (1988) examined the case in which all short waves regardless of their height are assumed to break at a fixed break point. This means that the groupiness outside the surf zone is transmitted into the surf zone where long-wave generation can take place. Schäffer (1993) merged the two extreme mechanisms into one hybrid analytical solution for the total long-wave envelope in which a parameter $\kappa$ is used to interpolate between the two extremes. He analyzed some of the effects of parameter variations. In these investigations the forcing was generated by weakly-modulated wave groups composed of two short wave components propagating in

the same direction, which made analytical solutions possible for the steady state situation. This simplification clearly does not hold on a natural beach with a full spectrum of directionally-spread waves.

In a companion paper, Reniers and Van Dongeren (1999) released the restriction of a bichromatic short wave forcing in a single direction and presented an analytical model which calculates the infragravity wave response to a directional spectrum of incident waves on a cylindrical beach. The results were compared to DELILAH (1990) data taken at the Field Research Facility (FRF) site near Duck, NC, USA.

In this paper a model-data comparison is made using a nonlinear numerical model SHORECIRC (Van Dongeren *et al.*,1994; Van Dongeren & Svendsen, 1997b) which is based on the quasi 3-D depth-integrated, shortwave averaged equations of mass and momentum. In §2 the model equations are presented. §3 describes the synthesis of the boundary conditions. In §4 a model-data comparison is performed for two selected days of the 1990 DELILAH campaign.

# 2 Model Equations

In this section, we will give an overview of the depth-integrated, time-averaged governing equations of the SHORECIRC model. For a more thorough derivation of these equations for the case of depth-uniform currents we refer to the procedure

given by Phillips (1977) and Mei (1983), and for the more general case of depth-varying currents to Putrevu & Svendsen (1991), Putrevu & Svendsen (1997, 1999) and Van Dongeren & Svendsen (1997b).

The equations which the model solves are the conservation of mass and momentum equations for the long waves. It concurrently solves the energy equation for the short waves and the roller which act as a wavedriver for the longer waves.

The conservation of mass equation is given by

$$\frac{\partial \overline{\zeta}}{\partial t} + \frac{\partial}{\partial x_\alpha}\left(\tilde{V}_\alpha\, h\right) = 0 \tag{1}$$

where $\overline{\zeta}$ is the surface elevation of the long (or IG) wave motion, $\tilde{V}_\alpha$ is the depth-averaged long wave velocity. The index $\alpha$ represents the horizontal $x$, $y$ directions. $z$ is the vertical coordinate, defined from the still water level (SWL) up. $h = h_o + \bar{\zeta}$ is the total depth, where $h_o$ is the still water depth. See Fig. 1 for a definition sketch.

After fairly lengthy derivations, the conservation of momentum equation can be written as

$$\frac{\partial}{\partial t}\left(\tilde{V}_\beta\, h\right) + \frac{\partial}{\partial x_\alpha}\left(\tilde{V}_\alpha\, \tilde{V}_\beta\, h + M_{\alpha\beta} + A_{\alpha\beta\gamma}\, \tilde{V}_\gamma\right)$$

$$-\frac{\partial}{\partial x_\alpha}\left[h\left(D_{\beta\gamma}\frac{\partial \tilde{V}_\alpha}{\partial x_\gamma} + D_{\alpha\gamma}\frac{\partial \tilde{V}_\beta}{\partial x_\gamma} + B_{\alpha\beta}\frac{\partial \tilde{V}_\gamma}{\partial x_\gamma}\right)\right]$$

$$+ g\,h\,\frac{\partial \bar{\zeta}}{\partial x_\beta} + \frac{1}{\rho}\frac{\partial S_{\alpha\beta}}{\partial x_\alpha} - \frac{\partial}{\partial x_\alpha}\left[h\,\nu_t\left(\frac{\partial \tilde{V}_\alpha}{\partial x_\beta} + \frac{\partial \tilde{V}_\beta}{\partial x_\alpha}\right)\right] - \frac{\tau_\beta^S - \tau_\beta^B}{\rho} = 0 \quad (2)$$

where $\beta$ is index notation for the horizontal $x$ and $y$ directions, $\nu_t$ is the turbulent eddy viscosity, $\tau_\beta^S$ is the surface stress and $\tau_\beta^B$ is the bottom stress. The radiation stress is defined as

$$S_{\alpha\beta} \equiv \overline{\int_{-h_o}^{\zeta} (p\,\delta_{\alpha\beta} + \rho\,u_{w\alpha}\,u_{w\beta})\,dz} - \delta_{\alpha\beta}\frac{1}{2}\rho\,g\,h^2 \quad (3)$$

where $\delta_{\alpha\beta}$ is the Kronecker delta.

The coefficients represent the depth-varying current-current and wave-current interaction terms and are defined as (see Putrevu & Svendsen (1997, 1999) for details)

$$D_{\alpha\gamma} \equiv \frac{1}{h}\int_{-h_o}^{\bar{\zeta}} V_{1\alpha}^{(0)} \int_z^{\bar{\zeta}} \frac{1}{\nu_t}\int_{-h_o}^{z} V_{1\gamma}^{(0)}\,(dz)^3 \quad (4)$$

$$M_{\alpha\beta} \equiv \int_{-h_o}^{\bar{\zeta}} V_{1\alpha}^{(0)}\,V_{1\beta}^{(0)}\,dz + V_{1\alpha}^{(0)}(\bar{\zeta})\,Q_{w\beta} + V_{1\beta}^{(0)}(\bar{\zeta})\,Q_{w\alpha} \quad (5)$$

$$\begin{aligned} A_{\alpha\beta\gamma} \equiv & -\int_{-h_o}^{\bar{\zeta}} V_{1\alpha}^{(0)} \int_z^{\bar{\zeta}} \frac{1}{\nu_t}\left(\frac{\partial}{\partial x_\gamma}\int_{-h_o}^{z} V_{1\beta}^{(0)}\,dz - V_{1\beta}^{(0)}\frac{\partial h_o}{\partial x_\gamma}\right)(dz)^2 \\ & -\int_{-h_o}^{\bar{\zeta}} V_{1\beta}^{(0)} \int_z^{\bar{\zeta}} \frac{1}{\nu_t}\left(\frac{\partial}{\partial x_\gamma}\int_{-h_o}^{z} V_{1\alpha}^{(0)}\,dz - V_{1\alpha}^{(0)}\frac{\partial h_o}{\partial x_\gamma}\right)(dz)^2 \end{aligned} \quad (6)$$

$$\begin{aligned} B_{\alpha\beta} \equiv & \frac{1}{h}\int_{-h_o}^{\bar{\zeta}} V_{1\alpha}^{(0)} \int_z^{\bar{\zeta}} \frac{1}{\nu_t}\int_{-h_o}^{z} V_{1\beta}^{(0)}\,(dz)^3 - \frac{1}{h}\int_{-h_o}^{\bar{\zeta}} V_{1\alpha}^{(0)} \int_z^{\bar{\zeta}} \frac{1}{\nu_t} V_{1\beta}^{(0)}\,(h_o + z)\,(dz)^2 \\ & -\frac{1}{h}\int_{-h_o}^{\bar{\zeta}} V_{1\beta}^{(0)} \int_z^{\bar{\zeta}} \frac{1}{\nu_t} V_{1\alpha}^{(0)}\,(h_o + z)\,(dz)^2 \end{aligned} \quad (7)$$

where $V_{1\alpha}^{(0)}$ is the depth-varying long wave velocity forced by the local external forcing (among others the radiation, bottom, and surface stresses), and $Q_{w\alpha}$ is the shortwave-induced volume flux.

The radiation stresses provide the shortwave forcing on these equations. The radiation stresses are calculated from the energy $E$ of the short waves and the roller energy $E_r$ as (Reniers, 1999)

$$S_{\alpha\beta} = 8\,P_{\alpha\beta}\,E + 2\,E_r\,\frac{k_\alpha\,k_\beta}{k^2} \tag{8}$$

where $k_{\alpha,\beta}$ are components of the wave number of the carrier short wave motion and $P_{\alpha\beta}$ is the nondimensional shape parameter for the short waves. Using sine wave theory for the short waves, the shape factor $P_{\alpha\beta}$ in (8) becomes

$$P_{\alpha\beta} = \frac{1}{16}\left[(1 + \frac{2\,k\,h_o}{\sinh\,2\,k\,h_o})\frac{k_\alpha\,k_\beta}{k^2} + \frac{2\,k\,h_o}{\sinh\,2\,k\,h_o}\,\delta_{\alpha\beta}\right] \tag{9}$$

The energy equation for the short waves (where the time scale is of the energy variation of the shortwaves follows from the Hilberttransform (envelope function) of the shortwave motion) can be written as

$$\frac{\partial E}{\partial t} + \frac{\partial}{\partial x_\alpha}\left(E_{f\alpha} + \tilde{V}_\alpha\,E\right) + S_{\alpha\beta}\,\frac{\partial \tilde{V}_\beta}{\partial x_\alpha} + \mathcal{D} + \tilde{V}_\alpha\,\tau_{b\alpha} = 0 \tag{10}$$

where $E_{f\alpha}$ is the energy flux and $\mathcal{D}$ is the dissipation is modelled as

$$\mathcal{D} = 2\,f_p\,E\,\frac{\frac{H}{h}}{1 - \left(\frac{H}{2\,h}\right)^2}\,\tanh\left[\left(\frac{H}{\gamma\,h}\right)^{10}\right] \tag{11}$$

The first part of this equation corresponds to the formula for bore dissipation (Svendsen, 1984a; Stive, 1984), while the hyperbolic tangent function represents the prob-

ability of breaking function proposed by Thornton & Guza (1983) and Roelvink (1993) but in a slightly different form.

The roller energy is solved from the time-varying version of the formulation derived by Nairn *et al.* (1999) and Stive & De Vriend (1994):

$$\frac{\partial E_r}{\partial t} + \frac{\partial}{\partial x_\alpha}\left(2\,E_r\,c\,\frac{k_\alpha}{k}\right) - \mathcal{D} + \mathcal{D}_r = 0 \tag{12}$$

where the dissipation of the roller is modelled as

$$\mathcal{D}_r = \frac{2\,g\,\sin(\beta)}{c}\,E_r \tag{13}$$

following Reniers (1999) where $\beta$ is the slope of the wave front.

In the version of the SHORECIRC model used here, the governing equations are solved using a central finite difference scheme on a fixed spatial grid with an explicit second-order Adams-Bashforth predictor and a third-order Adams-Moulton corrector time-stepping scheme.

# 3 Synthesis of Boundary Conditions

The rectangular computational domain (e.g., Fig. 7) in which the governing equations are solved has four boundaries. In the computational domain the origin is located at an offshore corner of the domain, with the $x$-axis positive shoreward and the $y$ axis along the offshore boundary of the domain.

At the landward side of the domain we impose a simple no flux boundary condition. On the lateral (shore-normal) boundaries we use a periodicity condition.

On the artificial, seaward boundary of the computational domain an absorbing-generating boundary condition is imposed. This boundary condition, which was described in detail in Van Dongeren & Svendsen (1997a), is capable of simultaneously generating incoming and absorbing outgoing waves with a minimum of reflection.

On the offshore boundary, the incoming shortwave energy (i.e., the boundary condition for (10)) and the associated flux of the incoming bound long wave (i.e., the boundary condition for (2)) are calculated from measured wind wave spectra. The procedure is as follows:

A wind wave spectrum measured at the FRF array in 8 meters of water depth was selected from the DELILAH data set (Birkemeier *et al.*, 1997), see Fig. 2. For this model-data comparison we selected the data recorded on October 10 and 13, 1990 both at 10:00 hrs. The wind wave spectra are fairly energetic ($H_{m0} = 1.14\,m$ and $H_{m0} = 2.18\,m$) and are narrow-banded in the frequency domain, which means that wave groupiness is pronounced and thus that the time-varying forcing on the time scale of the wave groups will be energetic as well. The measured spectra were reproduced from Birkemeier *et al.* (1997). The spectrum of October, 13 is shown in Fig. 3. In this figure an angle of zero degrees corresponds to shorenormal incidence in the SHORECIRC coordinate system. The angle is defined positive counterclockwise

in this coordinate system.

In the problem at hand, this measured swell spectrum represents the shortwave energy which is to be used as input in the energy equation (10). In order to calculate the shortwave energy on the basis of the measured spectra the spectrum is assumed to be composed of $K$ single-summation wave components in a range around the spectral peak where the energy density is larger than 10% of the peak energy density. Each wave component is defined by a frequency, amplitude, phase, and direction, and the summation over the number of components reads:

$$\zeta(0,y,t) = \sum_{i=0}^{K} A_i \cos(k_i \sin\theta_i \, y - 2\,\pi\, f_i \, t + \psi_i) \tag{14}$$

where

$$A_i = \sqrt{2\, E_i \, \Delta f \, \Delta\dot{\theta}} \tag{15}$$

and $E_i$ is found from the measured energy density distribution. In our simulations we chose $K = 100$. The phases $\psi$ are selected using the random phase method. The wavenumbers $k_i$ are calculated using the linear dispersion relation using the given depth of 8 $m$. The angles $\theta_i$ for every frequency $f_i$ are found from the probability function

$$P(\theta) = \int_{-\pi}^{\theta} D(\theta')\, d\theta' \tag{16}$$

where $D(\theta')$ is the spreading function (p.d.f.) at the peak frequency. In order to ensure periodicity, these angles $\theta$ are adjusted slightly such that for every component the alongshore wavenumber $k_i \sin\theta_i$ is an integer multiple of $\frac{2\pi}{L_y}$ where $L_y$ is the

alongshore length of the computational domain. Figure 4 shows the randomly-picked angles and the adjusted angles.

With the generated information, the wave field $\zeta(0, y, t)$ can be constructed along the offshore boundary $x = 0$. The comparison between the synthesized energy density spectrum and the measured spectrum in Fig. 5 shows that the lines coincide and all the energy around the peak is represented in the synthesized wave field.

The envelope of this wave field is calculated using the Hilbert transform. Fig. 6(a) shows an example of the synthesized time series and the envelope at the origin. From the envelope function we can determine the energy in the short wave as a function of time - using linear theory - as

$$E(0, y, t) = \frac{1}{2} \rho g A^2(t) \tag{17}$$

which is shown in Fig. 6(b) and will be used as a boundary condition on the energy equation (10).

In addition to the incident short wave field we also need to determine the incoming bound (second-order) low frequency waves associated with the short waves. The amplitude of the bound waves can be calculated from the theory developed by Hasselmann (1962) where we use a form similar to the one used by Herbers *et al.* (1994). The forced secondary wave with difference frequency $\Delta f$ is generated by two interacting short waves with frequencies $f$ and $f + \Delta f$. Note that a whole set of pairs of short wave components contribute to the forcing of a long wave component

with one particular difference frequency. The energy of the secondary forced surface elevation $E_f(\Delta f)$ can be computed following Herbers *et al.* (1994) as

$$E_f(\Delta f) = 2 \int_{\Delta f}^{\infty} \int_0^{2\pi} \int_0^{2\pi} D^2(f+\Delta f, -f, \Delta\theta+\pi)\, E(f+\Delta f, \theta_1)\, E(f, \theta_2)\, d\theta_2\, d\theta_1\, df \tag{18}$$

where $E(f,\theta)$ is the 2-D energy density of the primary-waves surface elevation, subscripts 1 and 2 refer to the two interacting primary waves, and $D(f+\Delta f, -f, \Delta\theta+\pi)$ is the difference-interaction coefficient with a difference angle $\Delta\theta = |\theta_1 - \theta_2|$. This interaction coefficient for the surface elevation energy is defined as (Herbers *et al.*, 1994)

$$\begin{aligned} D(-f_1, f_2, \Delta\theta+\pi) \equiv{}& \frac{g\, k_1\, k_2\, \cos(\Delta\theta+\pi)}{8\pi^2\, f_1\, f_2} \frac{\cosh(k_3\, h)}{\cosh(k_1\, h)\cosh(k_2\, h)} \\ & - \frac{g\,(-f_1+f_2)}{[g\, k_3\, \tanh(k_3\, h) - (2\pi)^2(-f_1+f_2)^2]\, f_1\, f_2} \\ & \times \left\{ (-f_1+f_2) \left[ \frac{(2\pi)^4\,(f_1 f_2)^2}{g^2} - k_1\, k_2\, \cos(\Delta\theta+\pi) \right] \right. \\ & \left. - \frac{1}{2} \left[ \frac{-f_1\, k_2^2}{\cosh^2(k_2\, h)} + \frac{f_2\, k_1^2}{\cosh^2(k_1\, h)} \right] \right\} \end{aligned} \tag{19}$$

Note that Herbers' formulation was applied to bottom pressures. In this equation the difference wave number is

$$k_3 \equiv |\vec{k_1} - \vec{k_2}| = \sqrt{k_1^2 + k_2^2 + 2\, k_1\, k_2\, \cos(\Delta\theta)} \tag{20}$$

The amplitude of the bound wave can be found from

$$A_{f,i} = \sqrt{2\, E_f\, df} \tag{21}$$

The bound wave is assumed to be in local equilibrium with the forcing from the interacting primary waves. This means that long wave is 180° out of phase with the sum of the two primary waves. The direction of the bound wave can be found from a geometrical consideration where

$$\theta_3 = \arctan\left(\frac{k_2 \sin\theta_2 - k_1 \sin\theta_1}{k_2 \cos\theta_2 - k_1 \cos\theta_1}\right) \tag{22}$$

From the calculated amplitude, phase and angle we can construct the time series of the bound long wave associated with the incoming short wave groups. The shore-normal volume flux of the bound long wave is shown in Fig. 6(c).

The time series of the envelope of the time-varying shortwave energy and the bound long wave serve as input into the model. Note that the incoming free long wave energy is not modelled although it may be present in the data.

# 4 Model-data comparison

## 4.1 October 10, 1990 at 10:00 hrs.

The nonlinear model is validated against two particular days of the Delilah (1990) campaign. The first selected day was October 10 (10:00 hrs) which was the day before the first major storm of the campaign. The wave heights were already significant. The model was run for a simulation time of one hour using the boundary conditions synthesized in the previous section. The model was compared to the

time series collected in the primary cross-shore array of pressure gauges and current meters CM/PD 10-90, which are shown in Fig. 7 and 8.

Fig. 9 (a) shows the comparison between the measured and computed $H_{rms}$ waveheights of the short waves in the primary cross-shore array. The wave height decay is predicted reasonably well, but the shoaling is underestimated. Panel (b) shows the measured and computed mean longshore currents. The overall agreement is very good; the maximum of the longshore current is located in the trough. Panel (c) shows the location of the primary cross-shore array relative to the bathymetry.

The model is not only capable of predicting the mean wave height and velocity but also the time-varying motion. Fig. 10 shows the measured (solid line) and computed (dashed line) frequency spectra at nine locations in the primary cross-shore array. Location CM10 is the most shoreward location, while CM90 is the most seaward. We see that the location of the peaks in the spectra is generally predicted well, but that the energy level is underestimated by the model. Also note that the model is not intended to simulate the motion near the peak frequency of the short wave motion (around $f_p = 0.1Hz$) and that the computed spectra drop off in that range. The range in which this model is expected to be valid is from the zero frequency to about half the peak frequency.

### 4.2 October 13, 1990 at 10:00 hrs.

A similar comparison was made for October 13 (10:00 hrs), which was a stormy day with significant wave heights of 2.18 $m$. Fig. 11 (a) shows the comparison between the measured and computed $H_{rms}$ waveheights in the primary cross-shore array. Again, the wave height decay is predicted reasonably well. Note that gauge CM60 (at about $x = 730\,m$ was not functioning at the time. Panel (b) shows the measured and computed mean longshore currents. The overall agreement is rather poor; the measurements show a strong longshore current in the offshore region outside the surf zone which indicates that there must have been an ambient current which cannot be predicted with the model. Panel (c) shows the location of the primary cross-shore array relative to the bathymetry.

Fig. 12 shows the measured (solid line) and computed (dashed line) spectra versus frequency at nine locations in the primary cross-shore array. Again the location of the two peaks in the low-frequency end of the spectrum are predicted fairly well, but the energy levels are too low.

## 5 Discussion

This concludes the progress report on this research. The next topics which will be addressed are the influence of the non-uniformity of the bathymetry, the effect of

the work term in the energy equation, and the comparison with the linear model by Reniers and Van Dongeren.

# 6 Conclusions

The nonlinear numerical model SHORECIRC (Van Dongeren *et al.*, 1994) is applied to simulate the infragravity wave conditions on October 10th and 13th during the 1990 Delilah campaign. The SHORECIRC model has been extended in this case and includes the time-varying shortwave energy and roller equations in order to model the short wave height transformation.

In order to simulate the wave conditions an algoritm has been derived which synthesizes a directional offshore wavefield from data including the bound, directional low-frequency components (based on theory by Hasselmann (1962) and Herbers *et al.*, 1994)), which serves as the boundary condition for the model.

The model-data comparison shows that the mean short wave transformation on the real bathymetry is predicted correctly, and that the mean longshore current is predicted very well for one of the two days without tuning the parameters. The measured longshore current for the other day shows large velocities outside the surfzone which indicates an ambient (i.e., nonlocally driven) current, which is not modelled.

The structure of the infragravity spectrum as measured in the nearshore array is correctly represented but the energy level is underestimated. The agreement is better for the first day than for the second day.

# 7 Acknowledgments

This work has been sponsored by the Netherlands Centre for Coastal Research (NCK), the National Institute for Coastal and Marine Management (RIKZ), Delft University of Technology, and WL|Delft Hydraulics.

# 8 References

Birkemeier, W.A., C. Donohue, C.E. Long, K.K. Hathaway, C.F. Baron (1997). "1990 DELILAH Nearshore Experiment: Summary Report." Technical Report CHL-97-24, U.S. Army Corps of Engineers, Waterways Experiment Station, Vicksburg, Miss., USA.

Chen, Y. and R.T. Guza (1998). "Resonant scattering of edge waves by longshore periodic topography." *J. of Fluid Mechanics*, *369*, pp. 91-123.

Chen, Y. and R.T. Guza (1998). "Resonant scattering of edge waves by longshore periodic topography: finite beach slope." *J. of Fluid Mechanics*, *387*, pp. 255-269.

Hasselmann, K. (1962). "On the non-linear energy transfer in a gravity-wave spectrum. Part I: General theory." *Journal of Fluid Mechanics, 12*, pp. 481-500.

Herbers, T.H.C., S. Elgar and R.T. Guza (1994). "Infragravity-frequency (0.005-0.05 Hz) motions on the shelf. Part I: Forced waves." *J. of Phys. Ocean., 24*, pp. 917-927.

Lippmann, T.C., R.A. Holman and A.J. Bowen (1997). "Generation of edge waves in shallow water." *J. of Geophys. Res., 112, C4*, pp. 8863-8879.

Longuet-Higgins, M.S. and R.W. Stewart (1962). "Radiation stress and mass transport in gravity waves with application to 'surf-beats'." *Journal of Fluid Mechanics, 8*, pp. 565-583.

Longuet-Higgins, M.S. and R.W. Stewart (1964). "Radiation stress in water waves, a physical discussion with applications." *Deep Sea Research, 11*, pp. 529-563.

Mei, C.C. (1983). *The applied dynamics of ocean surface waves.* John Wiley and Sons, New York, 740 pp.

Nairn, R.B., J.A. Roelvink, and H.N. Southgate (1990). "Transition zone width and implications for modelling surfzone hydrodynamics." *Proc. 22nd International Conference on Coastal Engineering*, pp. 68-81.

Phillips, O.M. (1977). *The dynamics of the upper ocean.* Cambridge University Press, 336 pp.

Putrevu, U. and I.A. Svendsen (1992). "A mixing mechanism in the nearshore region." *Proc. of the 23rd International Conference on Coastal Engineering*, pp. 2758-2771.

Putrevu, U. and I.A. Svendsen (1997). "Dispersive mixing in the nearshore." *Proc. Coastal Dynamics'97*, pp. 207-216.

Putrevu, U. and I.A. Svendsen (1999). "Three-dimensional dispersion of momentum in wave-induced nearshore currents." *European Journal of Mechanics, B/Fluids, vol. 18, no. 3, pp. 409-428.*

Reniers, A.J.H.M. (1999). "Longshore current dynamics." Ph.D. Dissertation, Communications on Hydraulic and Geotechnical Engineering, Fac. of Civil Engineering and Geosciences, Report no. 99-2, ISSN 0169-6548. 133 p.

Reniers, A.J.H.M. and A.R. Van Dongeren (1999). " ".

Rodi, W. (1980). *Turbulence models and their application in hydraulics.* Int'l Assoc. for Hydraulic Res., Delft, The Netherlands, 104 p.

Roelvink, J.A. (1993). Dissipation in random wave groups incident on a beach. *Coastal Engineering, 19*, pp. 127-150.

Sánchez-Arcilla, A., F. Collado, C. Lemos and F. Rivero (1990). "Another quasi-3D model for surf-zone flows." *Proc. of the 22nd International Conference on Coastal Engineering*, pp. 316-329.

Sánchez-Arcilla, A., F. Collado and A. Rodriguez (1992). "Vertically varying velocity field in Q-3D nearshore circulation." *Proc. of the 23rd International Conference on Coastal Engineering* , pp. 2811-2824.

Sancho,F.E., I.A. Svendsen and U. Putrevu (1999). "The effect on nearshore circulation of weak longshore topographic variations." *Submitted for publication.*

Schäffer, H.A. (1993). "Infragravity wave induced by short-wave groups." *J. Fluid Mech., 247*, pp. 551-588.

Schäffer, H.A. (1994). "Edge waves forced by short-wave groups." *J. Fluid Mech., 259*, pp. 125-148.

Schäffer, H.A. and I.A. Svendsen (1988). "Surf beat generation on a mild slope beach." *Proc. of the 21st International Conference on Coastal Engineering*, pp. 1058-1072.

Stive, M.J.F. (1984). "Energy dissipation in waves breaking on gentle slopes." *Coastal Engineering, 8*, pp. 99-127.

Stive, M.J.F. and H.J. de Vriend (1994). "Shear stresses and mean flow in shoaling and breaking waves." *Proc. 24th International Conference on Coastal Engineering.*, pp. 594-608.

Svendsen, I.A. (1984). "Wave heights and set-up in a surf-zone." *Coastal Engineering, 8*, pp. 303-329.

Svendsen, I.A. and R.S. Lorenz (1989). "Velocities in combined undertow and longshore currents." *Coastal Engineering, 13*, pp. 55-79.

Svendsen, I.A. and U. Putrevu (1990). "Nearshore circulation with 3-D profiles." *Proc. of the 22nd International Conference on Coastal Engineering*, pp. 241-254.

Svendsen, I.A. and U. Putrevu (1994). "Nearshore mixing and dispersion." *Proc. Roy. Soc. Lond. A., 445*, pp. 1-16.

Symonds, G., D.A. Huntley and A.J. Bowen (1982). Two dimensional surf-beat: Long wave generation by a time-varying break point. *Journal of Geophysical Research, 87, C1*, pp. 492-498.

Thornton, E.B. and R.T. Guza (1983). "Transformation of wave height distribution. " *J. of Geoph. Res., 88*, pp. 5925-5938.

Van Dongeren, A.R., F.E. Sancho, I.A. Svendsen and U. Putrevu (1994). "SHORECIRC: A quasi 3-D nearshore model." *Proc. of the 24th International Conference on Coastal Engineering*, pp. 2741-2754.

Van Dongeren, A.R. and I.A. Svendsen (1997a). "An absorbing-generating boundary condition for shallow water models." *Journal of Waterway, Port, Coastal and Ocean Engineering, 123*, no. 6, pp. 303-313.

Van Dongeren, A.R. and I.A. Svendsen (1997b). "Quasi 3-D modeling of nearshore hydrodynamics." *Research report CACR-97-04*, Center for Applied Coastal

Research, University of Delaware, Newark, 243 p.

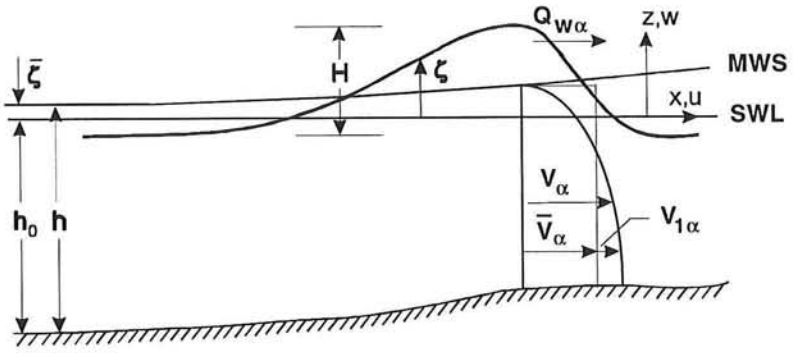


Figure 1: Definition sketch.

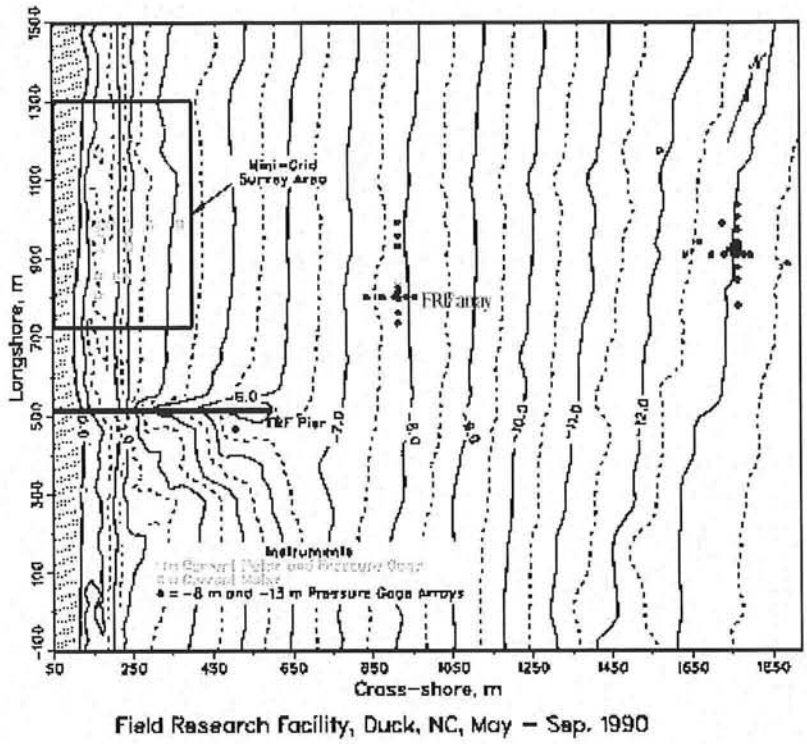


Figure 2: Plan view of the Field Research Facility at Duck, NC (USA).

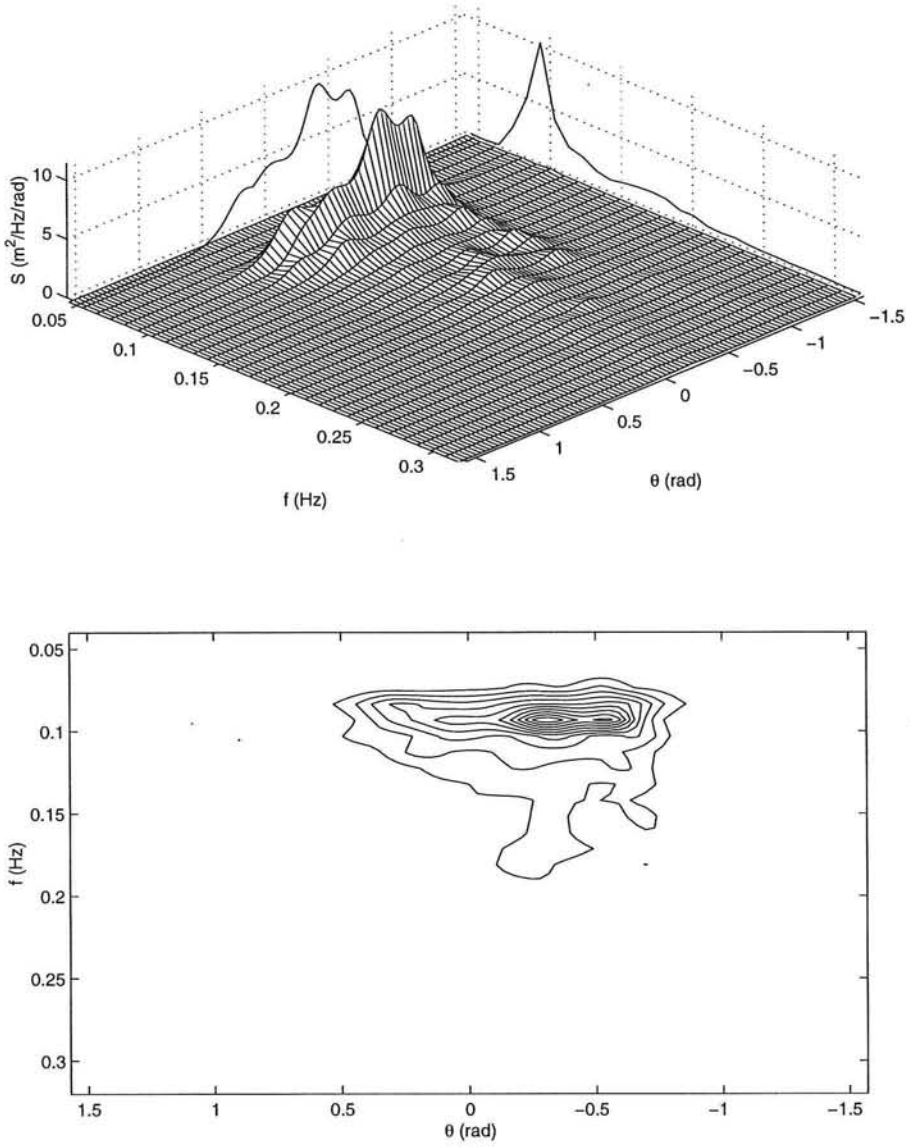


Figure 3: Directional spectrum measured at the FRF array (8 meters depth) on October 13, 1990 at 10:00 hrs. Top panel: surface plot; bottom panel: contour lines.

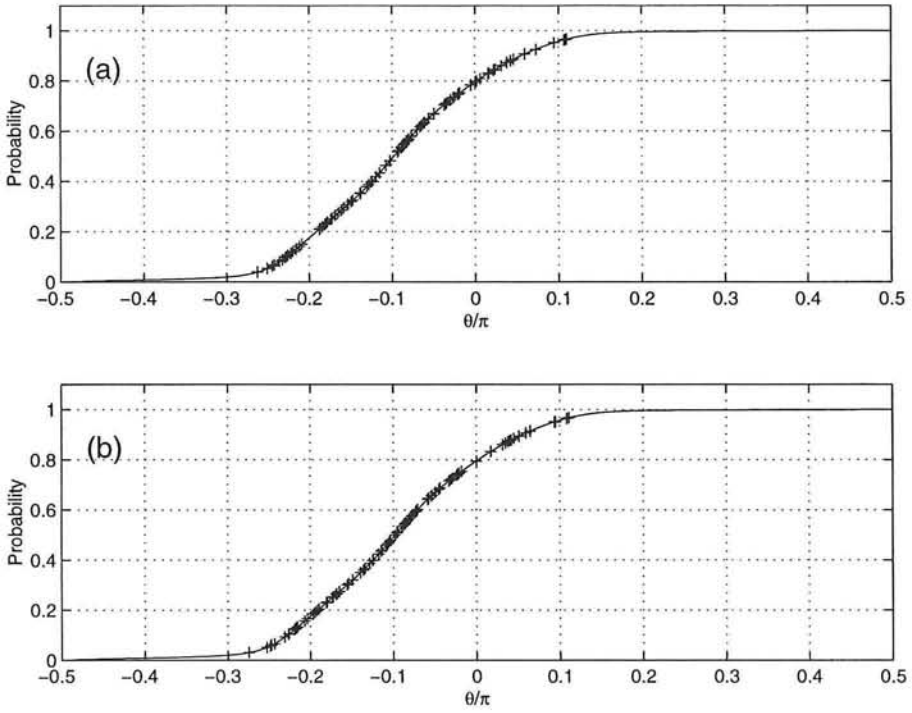


Figure 4: Top panel: Probability function vs. angle $\theta$ and randomly-selected angles. Bottom panel: Probability function and adjusted angles.

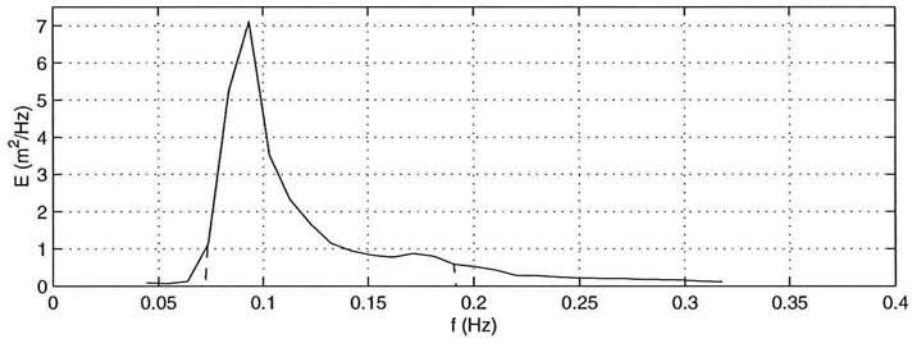


Figure 5: Measured energy density spectrum (solid line) vs. synthesized spectrum (dashed line).

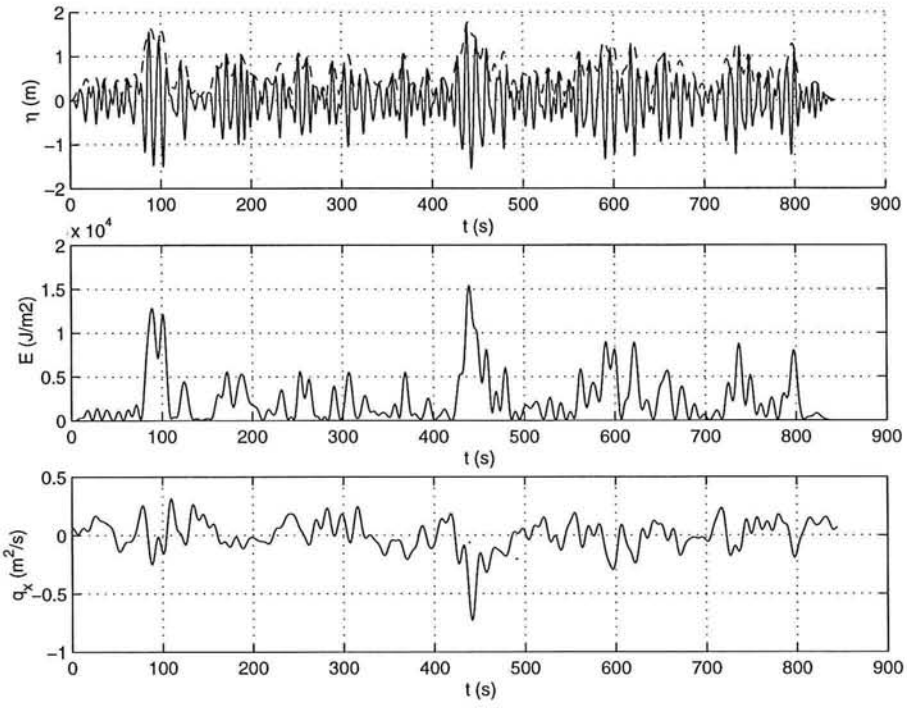


Figure 6: Top panel: Example of a synthesized surface elevation time series (solid line) and its envelope (dashed line). Middle panel: Time series of the shortwave energy. Bottom panel: Time series of the cross-shore volume flux of the bound wave.

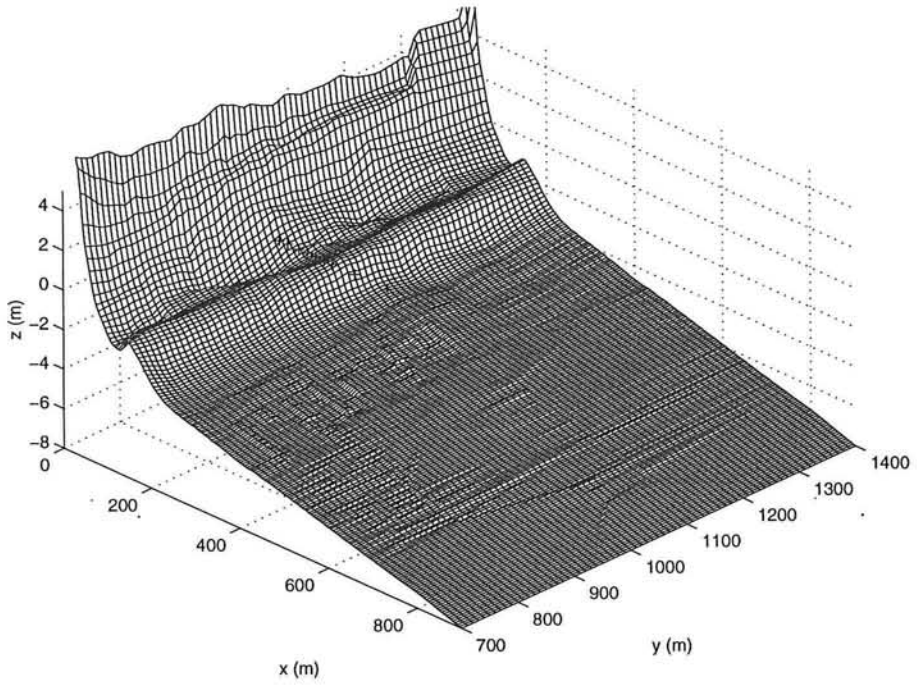


Figure 7: Bathymetry at Field Research Facility, measured on October 10, 1990 during the Delilah campaign. Axes in FRF coordinates. Also shown are the locations of the gauges in the primary cross-shore array.

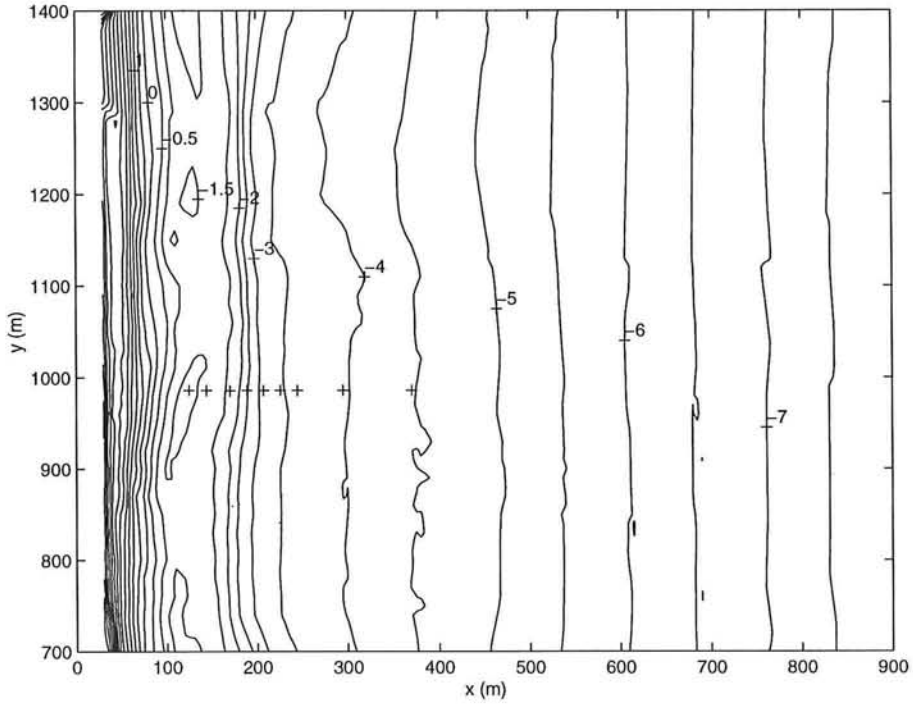


Figure 8: Contourlines of bathymetry at Field Research Facility, measured on October 10, 1990 during the Delilah campaign. Axes in FRF coordinates. Also shown are the locations of the gauges in the primary cross-shore array.

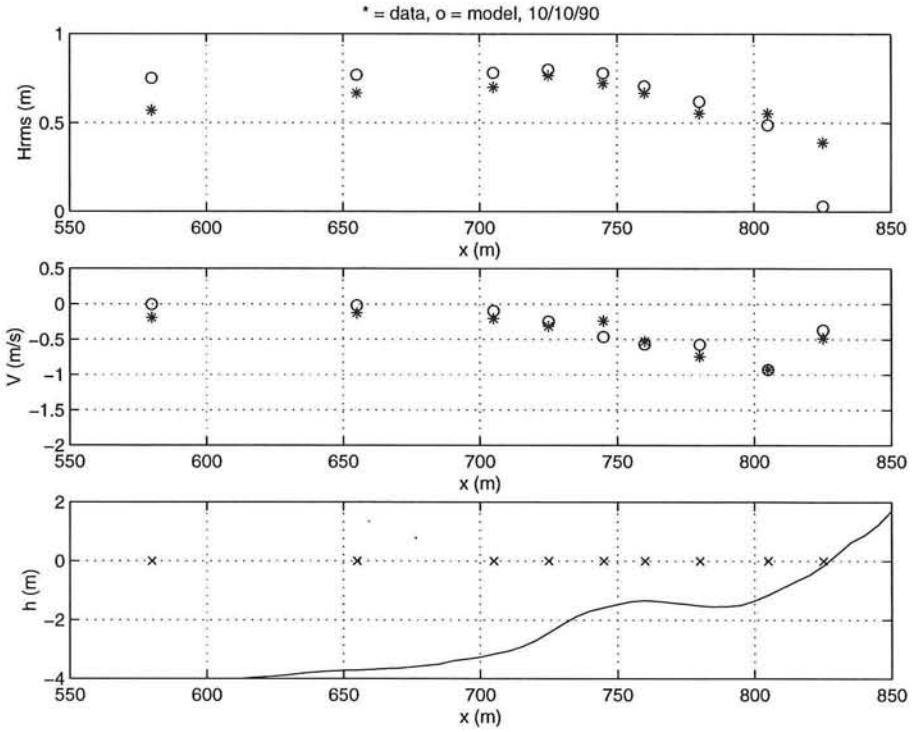


Figure 9: Measured (*) and computed (o) waveheights (panel a) and longshore currents (panel b) on October 10 at 10:00 hrs. Also shown is the cross-shore bathymetry and the locations of the instruments in the primary array.

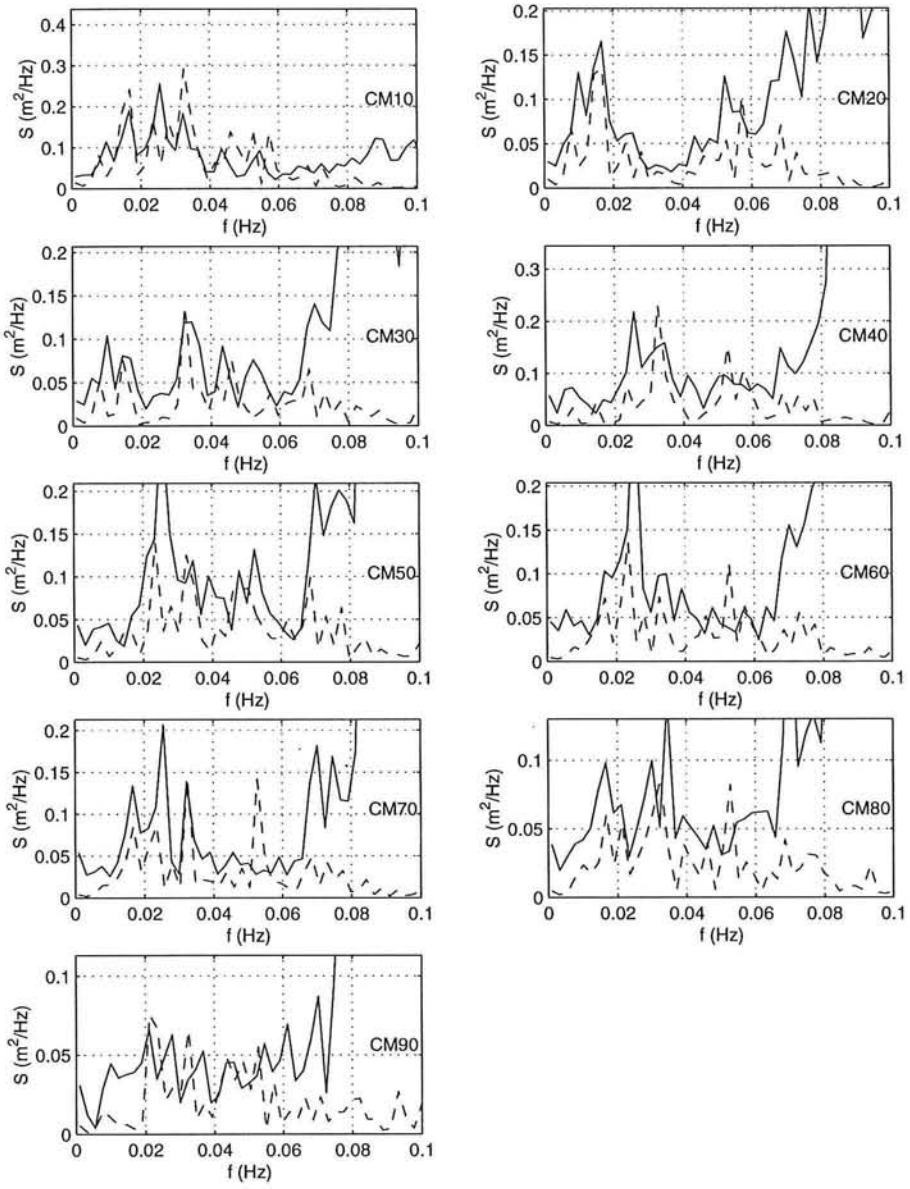


Figure 10: Measured (——) and computed (– –) surface elevation spectra on October 10 at 10:00 hrs for 9 locations in the primary cross-shore array, labelled in the panels. CM10 is the most shoreward gauge, CM90 the most seaward.

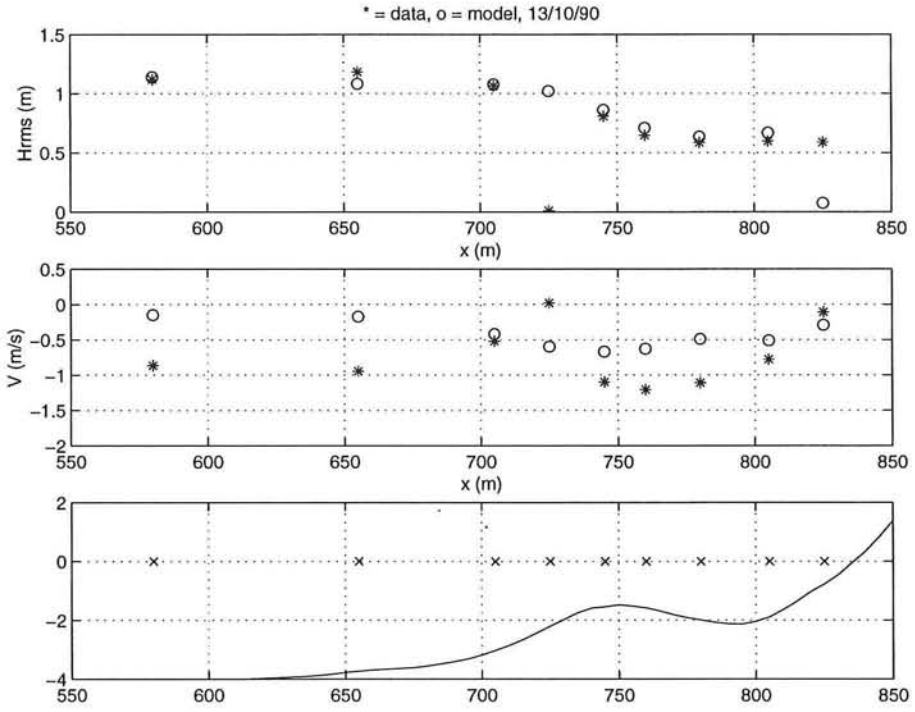


Figure 11: Measured (*) and computed (o) waveheights (panel a) and longshore currents (panel b) on October 13 at 10:00 hrs. Also shown is the cross-shore bathymetry and the locations of the instruments in the primary array.

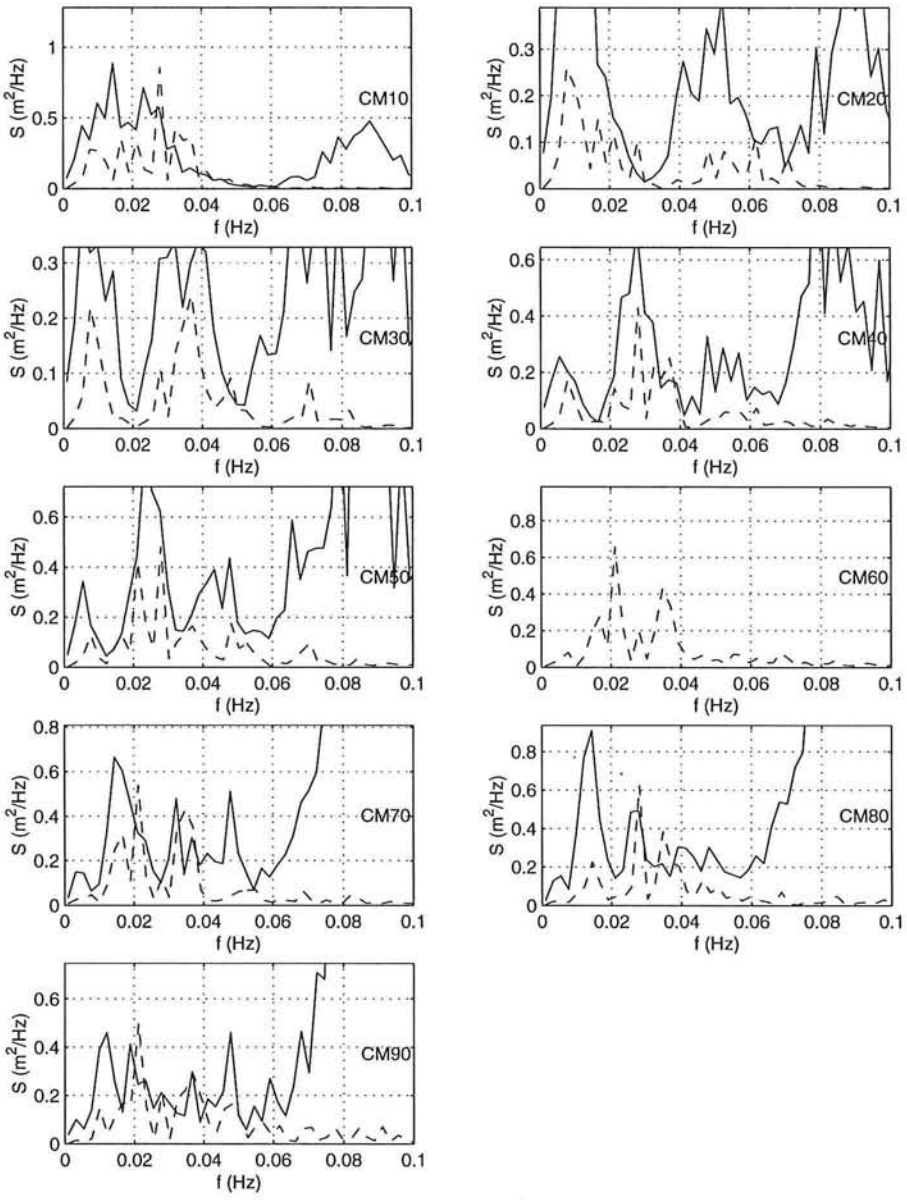


Figure 12: Measured (——) and computed (– –) surface elevation spectra on October 13 at 10:00 hrs for 9 locations in the primary cross-shore array, labelled in the panels. CM10 is the most shoreward gauge, CM90 the most seaward.